Thermal Conductivity of Thick Film Tungsten Metallization used in High-Alumina Ceramic Microelectronic Packages

Mark Eblen
Kyocera America, Inc.
8611 Balboa Ave.
San Diego, CA 92123
mark.eblen@kyocera.com

ABSTRACT

In a conventional high temperature co-fired multilayer 90~96% alumina microelectronic package, the thick film refractory metallization traces used for electrical signal routing also play a role in thermal conduction. This is seen in the electronics space with the common use of a thermal via array. What is less known is the quantitative thermal dissipation improvement due to the metallization. Answering this question poses experimental challenges as the co-fired metallization properties cannot be measured independently due to the sintering process interaction with the ceramic body. A quick inspection of the metallization electrical resistivity or sheet resistance when compared to that of pure tungsten provides evidence of this dramatic change in physical properties. Therefore, we are constrained to characterize the entire metallization/ceramic composite in a more or less homogenized manner. In the present study, directional normal and in-plane thermal diffusivity measurements were conducted on a geometrically simple periodic laminate metallization/alumina structure. The rear surface transient temperature response curve was then correlated to a finite element model by varying the metallization thermal conductivity until the low frequency component of the residual error was minimized.

INTRODUCTION

The first co-fired multilayer ceramic substrates were developed by RCA more than forty years ago. Modern multilayer 90~96% high alumina (Al_2O_3) microelectronic packages have steadily evolved becoming highly integrated systems comprising numerous semiconductor devices. A modern x-band fully integrated radar transmit and receive (T/R) module package is shown in Figure 1 [1]. Depending on the electrical routing complexity, package substrates can consist of up to twenty ceramic tape layers. These layers can range in thickness from .08 to .4 mm. Between each tape layer is a thick film refractory metallization that provides the electrical circuitry. Only tungsten metallization will be discussed in this study but molybdenum is also commonly used. In order to provide subject matter context, an abbreviated version of the manufacturing process for multilayer co-fired ceramic packages is provided.

The process begins with green processing of the tape cast ceramic sheets. The pliable “green” sheets consist of alumina ceramic, glass powder, and plasticizers mounted in a stainless steel frame for latter feature alignment. The sheets are screen printing with metallization paste forming the electrical conductor pattern. Sheets are electrically connected above or below by metallization filled barrel structures called via's. The individual sheets are pressure laminated and then heated to temperatures above 1500°C in a slightly wet H_2/N_2 atmosphere. The exposed surface metallization in the now “co-fired” monolithic ceramic body will be nickel plated (electroless and/or electrolytic) in preparation for subsequent brazing and/or soldering to metal components forming the microelectronic package. These thermal expansion matched metals can consist of integrated heat spreaders for thermal dissipation, perimeter leads for electrical connection, or seal rings for hermetic laser welding metal lid attach. A final electroless gold plating step is done to inhibit oxidation and corrosion.

Fig. 1: T/R Module Package Courtesy of EADS Astrium [1]

The genesis for this research was to quantitatively answer the fundamental question, "will this microelectronic package need an integrated heat spreader for thermal dissipation?" In order to answer this question, a comparison must be sought evaluating the semiconductor device junction temperature if attached to a metal (i.e. integrated spreader) or directly hard soldered onto a ceramic substrate. Additional considerations such as mechanical reliability must also be considered and have been discussed elsewhere [2].

In order to improve the thermal dissipation, a fine array of thermal vias transversing the substrate, centrally located under the die is usually provided during routing layout. A conventional thermal via array is shown in Figure 2. Obviously, the thermal conductivity (TC) of the co-fired metallization forming the via geometry will be of great interest to the thermal analyst during the preliminary design phase. A quick inspection of the metallization electrical resistivity or sheet resistance when contrasted with elemental tungsten provides evidence of a dramatic physical property change. This can be reconciled by considering the metallization/ceramic interface adhesion mechanism which has been explained by the glass penetration theory [3]. During co-firing, the green tape glass powder melts forming a liquid-phase between the alumina grains that penetrates the porous fine-grained metallization. During cooling, the liquid solidifies forming a dense metal-glass composite. A typical co-fired via microstructure is shown in Figure 3. Energy-dispersive x-ray spectroscopy mapping of the interfacial region would reveal no diffusion or reaction of tungsten with the fired alumina ceramic body. This may not be the case with other ceramic materials such as aluminum nitride (AlN).

FIRST ORDER TC APPROXIMATION

In a metallic solid, electrons are mainly responsible for transfer of heat. It is also known that the best electrical conductors are also the best thermal conductors. This proportional relationship is stated in the Wiedemann-Franz law, where the ratio of a materials thermal conductivity to electrical resistivity (σ) is equal to the product of the Lorentz number (L_o) and absolute temperature [4]. It should also be noted that L_o is nearly constant for most metals and approximately nearly equal to the Sommerfeld of 2.45E-8 W-Ω/K^2. The

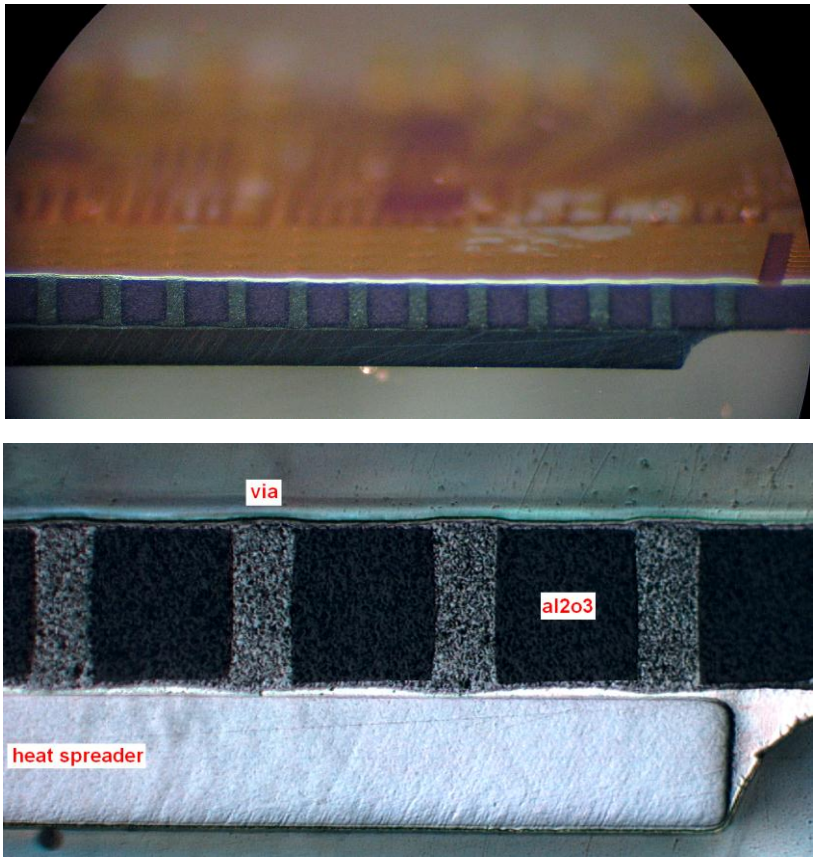

Fig. 2: Ceramic Package Thermal Via Array Micro-Section.

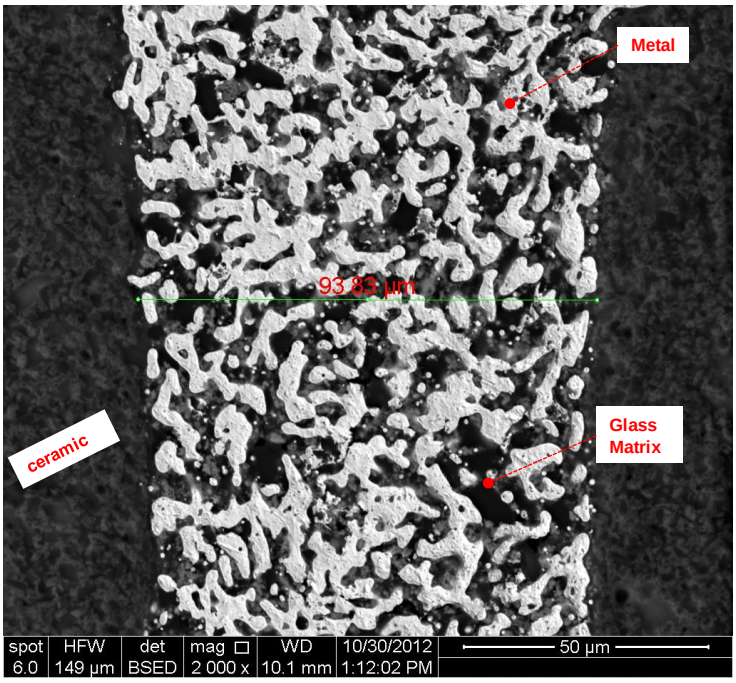

Fig. 3: SEM Image of a Conventional Co-Fired Metallization Microstructure.

Wiedemann-Franz (WF) law was derived from the kinetic theory of gases applied to solid-state physics.

In microelectronic packaging, the metallization electrical resistivity (or sheet resistance) is a common material property that is always included in supplier design guidelines. This fact, along with the above proportionality law, can be exploited in order to provide a first-order estimate of the tungsten metallization thermal conductivity. Recall that the metallization is not a pure metal but a metal-glass composite. For completeness, we will also append the Wiedemann-Law with a phonon conduction contribution term shown below in Equation 1.

$$k_{\text{total}} = k_{\text{electron}} + k_{\text{phonon}} \tag{1}$$

Where k_{total} is the total thermal conductivity using the thermal sciences notation, k_{electron} is the electronic contribution arising from the WF law and k_{phonon} is the smaller lattice contribution from elementary kinetic theory [5]. In Equation 2 the c_{vol} is the glassy phase heat capacity, ν is the propagation velocity, and λ is the electron mean free path. As a first order estimate we can assume the primary glassy phase composition is SiO_2 with an upper limit thermal conductivity value of approximately 1.3 W/m-K. As expected, this is negligible when compared against the dominate electronic contribution and can be neglected.

$$k_{\text{total}} = L_o \times \sigma \times T + \frac{c_{\text{vol}} \times \nu \times \lambda}{3} \tag{2}$$

$$k_{total} = 89 \frac{W}{mK} \tag{3}$$

Equation 2 can now be solved using vendor provided electrical resistivity data along the Lorentz constant for pure tungsten. The calculated value in Equation 3 will provide the basis for the subsequent experimental validation.

APPLICATION OF THE LASER FLASH METHOD

Thermal characterization techniques for solid materials can be divided into two broad categories, steady-state and transient, depending on the whether a time vs. temperature dependency exists [6]. Measurement of thermal conductivity has an inherit difficulty that it is a derived quantity and not measured directly. Another difficulty is the fact that thermal conductivity of most solids ranges only five orders of magnitude. This can be compared with the approximately fifteen orders of magnitude for electrical conductivity. As a result most solids have some ability to conduct heat; often complicating maintaining a mathematically correct temperature gradient during the experiment. This difficulty can be mitigated with the use of transient techniques, that by their very nature have a short measurement time. Thus, the heat losses will have a smaller, but not negligible, influence on the measurement.

All transient conduction measurement theory starts with solving the partial differential heat diffusion Equation 4 for a materials temperature gradient versus time. This equation is derived from an energy conservation approach combined with substitution of Fourier's proportional law for thermal conductivity. Further simplification can be had for one dimensional heat flow, homogeneity, isotropic properties, etc. This simplification is shown as Equation 5. The transport property thermal diffusivity (Eq. 6) enters into the theory as the ratio of thermal conductivity (k) over the product of the materials density and heat capacity (i.e.

volumetric heat capacity). Thermal diffusivity represents the propagation of heat into a solid body versus time and is the unknown quantity that is sought during a transient measurement. A larger thermal diffusivity, equates to more rapid response to heat flow. Thermal conductivity can be determined from Equation 6 if the volumetric heat capacity is known a priori.

$$\nabla \times \left(k \nabla T\right) + q''' = \rho \times c_p \frac{\partial T}{\partial t} \tag{4}$$

$$\nabla^2 T = \frac{1}{\alpha} \frac{\partial T}{\partial t} \tag{5}$$

$$\alpha = \frac{k}{\rho \times c_p} \tag{6}$$

For the present investigation, a transient method will be employed; commonly referred to as the laser flash method [7]. This approach was first proposed by Parker et al. [8] and consists of instantaneously irradiating a planar slab surface via laser pulse and then monitoring the rear face temperature vs. time evolution. The non-dimensional exponential series solution for this one dimensional temperature evolution takes the following form [9].

$$\frac{T(L,t)}{T_{\max}(L,t)} = 1 + 2\sum_{n=1}^{\infty} (-1)^n \exp\left(\frac{-n^2 \pi^2 \alpha t}{L^2}\right) \tag{7}$$

Diffusivity values can be calculated from the times required to reach a given percent rise of the response curve. The original Parker methodology used the convenient half-time ($t_{1/2}$) but other discrete rise times can be derived requiring only a change in the percent rise time constant [10].

$$\alpha = \frac{.1388 \times \mathrm{L}^2}{\mathrm{t}_{1/2}} \tag{8}$$

The modern, and more accurate, methodology relies on a nonlinear curve fit of the entire measured waveform to Equation 7 solving for the diffusivity. The following experimental conditions must remain valid during the measurement.

1. 1D heat flow through sample.
2. Adiabatic surfaces.
3. Uniform laser pulse absorption.
4. Short pulse duration vs. response (finite pulse effects).
5. Absorption of the pulse energy in a very thin layer.
6. Homogeneity and isotropy of the sample.
7. Constant transport and thermodynamic properties.

As was discussed earlier, it is not possible to physically separate the co-fired metallization from the ceramic body in order to measure each material's thermal diffusivity discretely. Therefore, we must conduct measurements using what can be referred to as an alumina/metallization periodic composite. Two distinct sample geometries were fabricated and measured, one in a through (or normal) direction to the metallization planes and one in the in-plane direction. Both directions are shown conceptually in Figure 4. Application of the laser flash method to these sample geometries will be discussed in the subsequent sections.

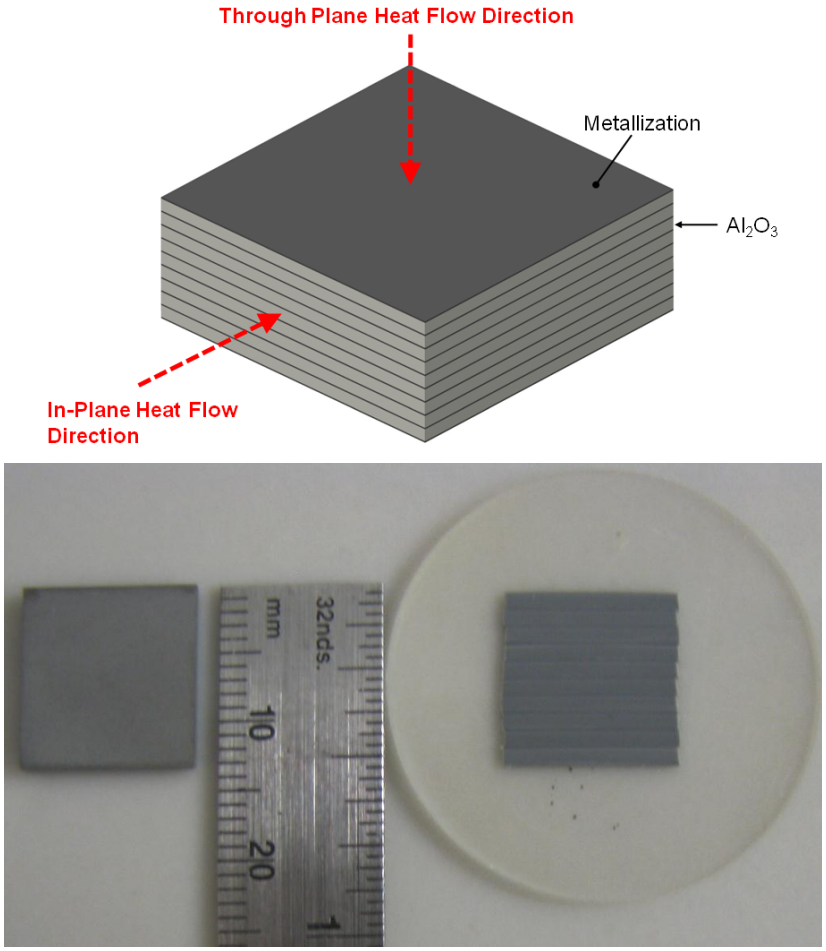

Fig. 4: Thermal Diffusivity Sample Geometry.

EXPERIMENTAL DESCRIPTION

Shown in Figure 5 is the custom laser flash system used in this study. The pulsed heat source consists of a 10.6 μm wavelength ten joule CO_2 laser. The approximately one-inch square beam is then attenuated through various thickness CaF_2 lenses and directed onto the sample through three copper mirrors. Two Au plated off-axis parabolic collecting mirrors focus the evolved thermal radiation from the sample's back surface onto the LN_2 cooled photoconductive HgCdTe detector with a 7 mm diameter viewing aperture. Detector biasing is done thru a bridge circuit. The optical path is contained in a polycarbonate custom

enclosure for operator safety. The sample is isolated from the aluminum fixture thru the use of a urethane gasket. Measurement samples that do not have a naturally high emissivity or absorptivity are coated with a thin layer of colloidal graphite spray. The high emissivity coating increases the energy absorption on the laser side and subsequent thermal radiation on the sample's back-surface. A pyroelectric joulemeter is used to trigger the LeCroy 6810 waveform recorder. The temperature vs. time waveform is digitized into 1024 data points before and 3072 data points after the laser pulse. A number of waveforms can then be averaged. The analysis program then calculates thermal diffusivity by two different methods. First, matching theory with experiment at $t_{1/4}$, $t_{1/2}$, and $t_{3/4}$ percent rise times. Next, a nonlinear least squares regression of the experimental waveform to the first four terms of the exponential series expression in Equation (7). Goodness-of-fit statistics are displayed allowing for a comparison of the fit and residual error with the theoretical model. Additional details can be found elsewhere [11].

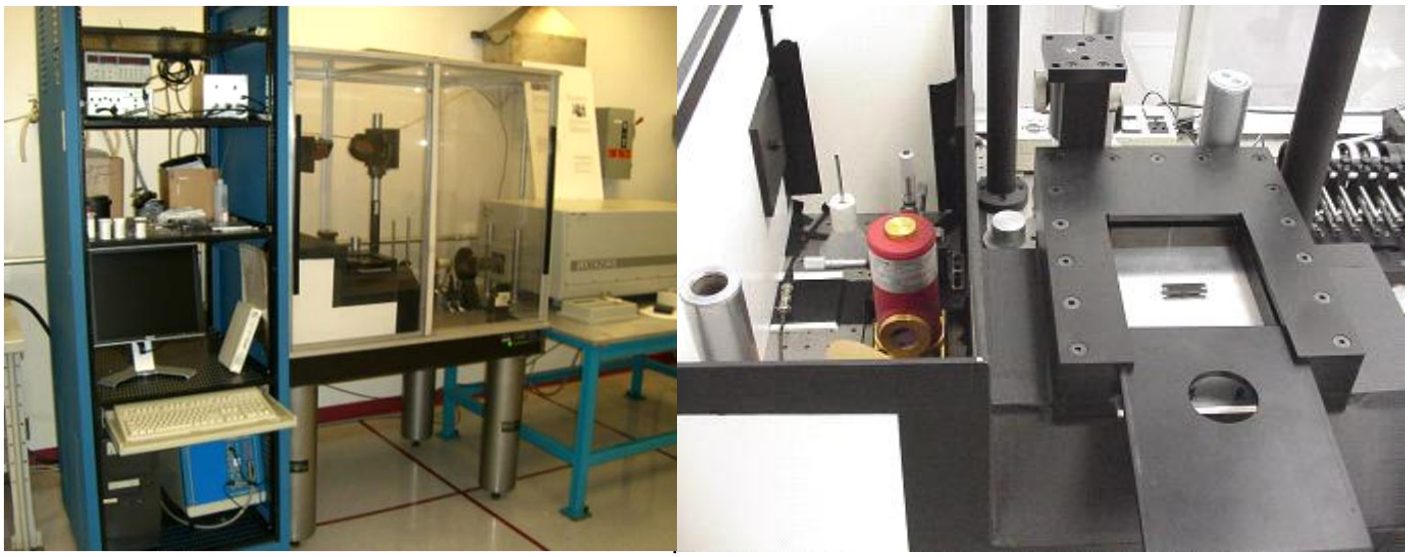

Fig. 5: Custom Laser Flash Experiment Setup used in Thermal Diffusivity Measurements.

THERMAL DIFFUSIVITY MEASUREMENTS

In the present study, normal and in-plane thermal diffusivity measurements were conducted on a geometrically simple periodic laminate metallization/alumina structure (refer Figure 4). The multilayer sample geometry consists of ten approximately 12.7 μm thick tungsten metallization layers and nine 127 μm thick 92% alumina ceramic layers. Co-fired nominal thickness was verified through metallurgical micro-sectioning and scanning electron microscopy measurements at numerous locations. The in-plane sample geometry was fabricated from precision diced 0.8 mm sections, oriented such that the tungsten metallization planes were parallel with the heat flow, then potted in epoxy and lapped down to the final thickness.

The density and specific heat capacity of the metallization must be measured separately in order to determine the metallization thermal conductivity. The effective composite density was determined via hydrostatic weighing. Once this thermodynamic property was measured, the metallization density could be calculated from a volume fraction rule-of-mixtures using Equation 8. The 92% alumina (Al_2O_3) properties were characterized from previous studies and remained invariant down to a thickness of 127 μm. The composite effective heat capacity was determined using a TA Instruments modulated differential scanning

calorimetry. The tungsten metallization heat capacity was calculated similarly using Equation 9. It should be understood that only the product of the two enters into the measurement theory.

$$\rho_{eff} = \rho_W \times \nu_w + \rho_{Al_2O_3} \times \nu_{Al_2O_3} \tag{8}$$

$$c_{eff} = \frac{c_W \times \rho_W \times \nu_W + c_{Al_2O_3} \times \rho_{Al_2O_3} \times \nu_{Al_2O_3}}{\rho_W \times \nu_W + \rho_{Al_2O_3} \times \nu_{Al_2O_3}} \tag{9}$$

Normal Diffusivity Measurement Results

Thermal diffusivity measurements of a laminate geometry with a thin thermally conductive layer on a thicker low conductivity substrate tend to have a great deal of uncertainty using the laser flash method [12]. Unfortunately, the present geometry used is expected to fall into this category as the ratio of metallization to alumina TC is estimated to be approximately five with thickness ratio being 0.1. Mathematical theory can help provide bounds on the measurement uncertainty. Taking an energy balance of a simpler limiting case consisting of a metallization layer attached to a thicker alumina layer. The derivation details will be omitted here for brevity but can be found in [13]. The effective diffusivity of the two layer structure with the metallization layer (W) receiving the heat pulse is given by the following:

$$\alpha_{eff} = \frac{L_{total}^2}{\frac{L_W^2}{\alpha_W} + \frac{L_{Al_2O_3}^2}{\alpha_{Al_2O_3}} + \frac{2L_W L_{Al_2O_3} \rho_{Al_2O_3} c_{Al_2O_3}}{\alpha_W \rho_W c_W}} \tag{10}$$

A plot of this differentiated equation holding the metallization diffusivity as constant demonstrates that for a typical five percent uncertainty in the effective diffusivity we cannot determine the metallization conductivity with any precision ≥ 35 W/mK. Clearly this approach will not prove successful if we anticipate the metallization TC value determined previously using Wiedemann-Franz law. As confirmation, a 1D finite element (FE) model of the ten layer normal sample was compared against measurement data. Details of the finite element thermal model will be discussed later in this report. The metallization TC was varied in the FE model and then compared against the measured transient response. This is shown in Figure 6 and confirms the previous theoretical treatment that a metallization TC slightly greater than 35 W/mK is not obtainable with this sample geometry. Decreasing the ceramic layer (tape) thickness would improve the situation but is not feasible due to manufacturing considerations. Therefore, another experimental approach must be sought.

In-Plane Diffusivity Measurement Results

The sample will now be oriented with the metallization planes parallel to the heat flow path providing a directional composite structure (Fig. 4). The conventional approach is to treat the constituents as a homogeneous material solving for an "effective" diffusivity. This continuum concept presumes all materials contain some level of heterogeneity; which when smaller that a critical size will behave as a homogeneous material. The effective diffusivity derived is usually some form of a weighted average of the constituent diffusivities. The unknown metallization TC (k_W) is then got from substitution of Equations 8-9, along with

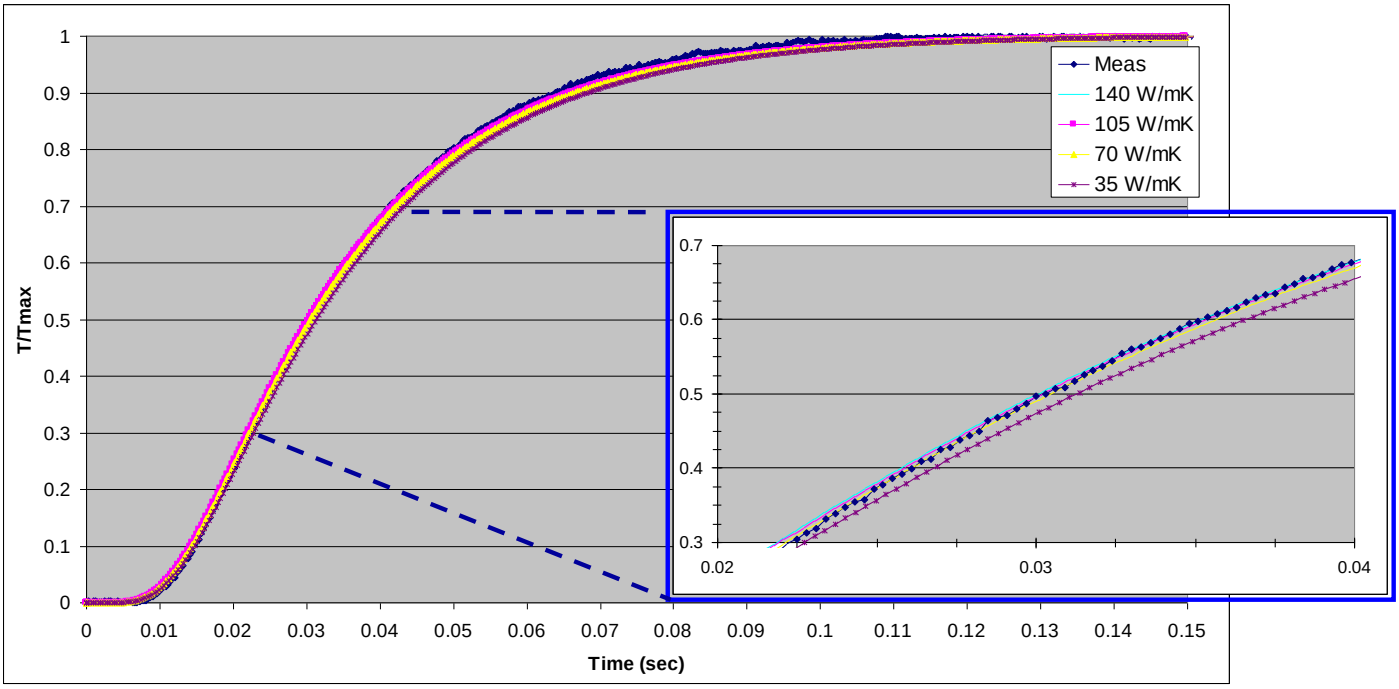

Fig. 6: Normal Diffusivity Measurement Results.

Equation 11 into Equation 6. Equation 11 is derived from a thermal resistances-in-parallel steady-state approximation for the effective or homogenized conductivity.

$$k_{eff} = \frac{k_W \times t_W + k_{Al_2O_3} \times t_{Al_2O_3}}{t_W + t_{Al_2O_3}} \tag{11}$$

Mathematically, this approach can be questionable, as the thermal diffusivity in Equation 4 is not coordinate independent. In practice however, this homogenized approach has been successfully applied to measurement of directional fiber reinforced composites [14]. Limits on the application of this technique are based on several size criteria put forth by Taylor [15] and Balageas et al [16]. They found the homogenized thermal behavior dependent on three governing parameters: the volume percentage of components, ratio of thermal diffusivities, and thermal contact conduction at the material interface. In addition, as the sample thickness becomes large compared to the reinforcing materials spacing the homogenized approach becomes a closer approximation. That is to say, the constituent materials are allowed to be thermally coupled. A more rigorous approach would be to find an analytical solution to the problem eliminating the uncertainty associated with the homogenized model. A closed-form analytical solution to this problem using Laplace transforms and separation of variables in cylindrical coordinates has been attempted in the literature and proved not possible [17-18]. A periodic unit structure description of the mathematical problem is shown in Figure 7. If we neglect the *x* coordinate direction thermal gradient, then a set of coupled differential equations can be derived [19]. Given the complicated summation series equations derived, they would prove very difficult to solve numerically. Again, we turn to a more general approach using the finite element method. Details of the model will be discussed later in Section 6 this report. The metallization TC was varied in the FE model and then compared against the measured transient response. It is immediately

apparent upon inspection of Figure 8, that this orientation provides good measurement fidelity in determining the metallization conductivity. This should be contrasted with the previous "normal" diffusivity measurements. While not shown in Figure 8 for clarity, a homogenized model assuming a best fit metallization TC value of 93 W/mK was also evaluated.

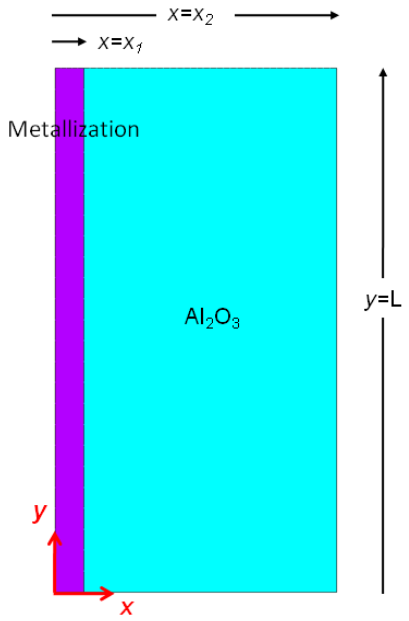

Fig. 7: In-Plane Diffusivity Unit Pitch Mathematical Model.

A good approximation was had using this approach. As mentioned previously, increasing the thickness of the sample tends to favor the homogenized approach. Therefore, another sample was prepared with a smaller thickness of 0.66 mm. These results are summarized below in Table 1 for comparison. The best fit values from the FE model were determined by minimizing the low frequency component (LF) of the root-mean-square (RMS) residual error. An initial detector pulse spike truncation routine was applied to the measured response and also included in the LF error determination.

Sample #	thickness (mm)	Best Fit TC (W/mK)	LF Error (%)	Homogenized LF Error (%)	% Diff.
17	0.841	104	0.170	0.181	6.3%
19	0.660	93	0.195	0.209	7.2%

Table 1: In-Plane Diffusivity Measurement Results.

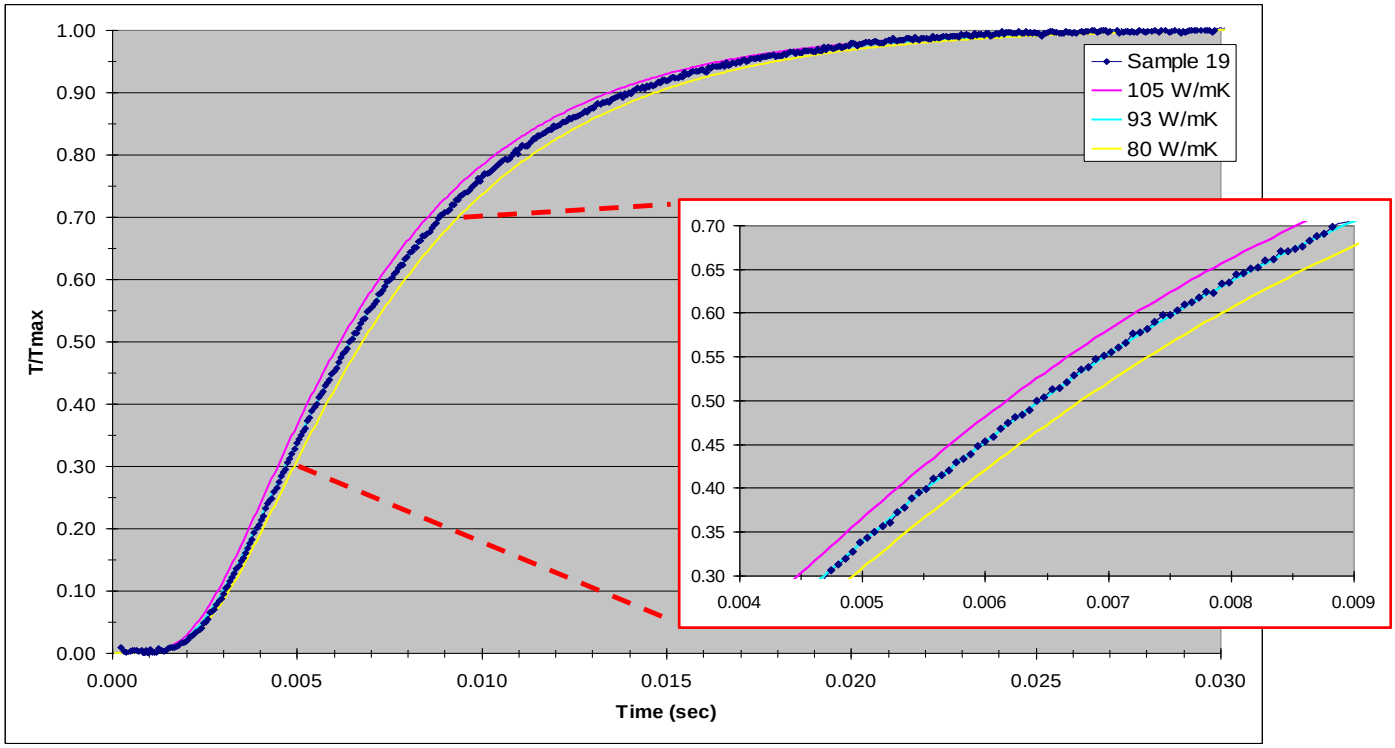

Fig. 8: In-Plane Diffusivity Measurement Results. 0.841 mm Sample Thickness

In-Plane Diffusivity Methodology Validation

As a technique validation, a control study was also conducted using well characterized industry materials. Following the same fabrication methodology used previously, a 0.51 mm thick 13/73/13 ratio copper-molybdenum-copper (CMC) symmetric metal laminate heat spreader was measured (Figure 9). The independent variable was copper with a final in-plane sample thickness of 0.5 mm after lapping. The best fit TC value was 391 ± 2 W/mK for the oxygen free high conductivity (OFHC) copper This value was very close to the vendor recommended 389 W/mK. Thus, the technique was considered valid for these types of periodic composites.

FINITE ELEMENT MODEL

In the present work, two transient thermal finite element models were created using commercially available software [20]. Both meshed models are shown in Figure 10. In order to keep computation time at a minimum, a 1D model was used for the through plane laminate model while a 2D periodic unit structure was exploited for the in-plane composite model. The in-plane model assumed an ideal interface between the materials (i.e. infinite contact conductance). All external surfaces were assumed adiabatic. The adiabatic assumption was validated by comparing results with and without a constant 10 W/m^2K average convective boundary condition applied to the top/vertical sides. The calculated thermal conductivity values were essentially the same for both these models. Other researchers have concluded the same [21]. The top irradiated surface was subjected to an instantaneous uniform heat flux. The instantaneous heat pulse assumption is reasonable considering the CO_2 laser used in this investigation has a pulse width of

approximately 10 µs which is well below 1% of the measured half rise time for these samples. The true pulse shape from this type of laser has an initial gain-switched spike around 200 ns full width half maximum and a longer exponential decay tail stretching out to 10 µs [22].

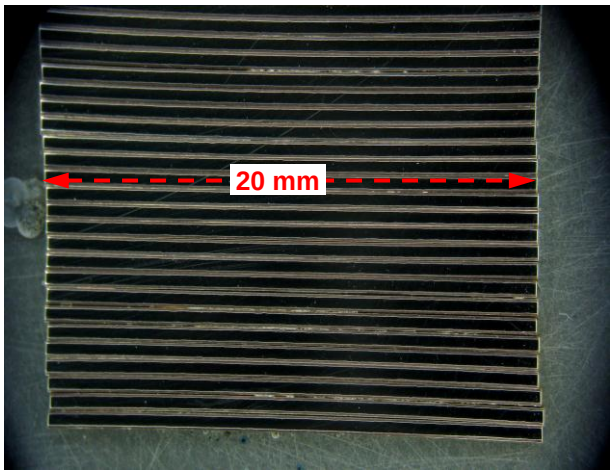

Fig. 9: 0.51 mm thick 13/73/13 CMC In-Plane Diffusivity Technique Validation Sample.

The time step and mesh size were judiciously chosen for numerical stability based on the following Equation 12 criteria. Keeping with convention, alpha is the material's thermal diffusivity. A logical start for the time step selection is the channel separation for the measured digitized data. This choice allows for a measured/simulated point by point error analysis without need for further non-linear curve regression.

$$\frac{\Delta \text{time}}{(\text{element length})^2} \geq \frac{.25}{\alpha} \tag{12}$$

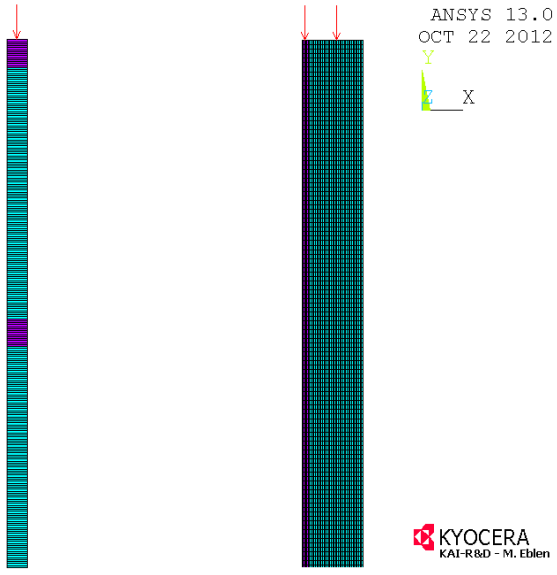

Fig. 10: Through Plane (left) and In-plane (right) Finite Element Transient Thermal Models.

CONCLUSIONS & FUTURE WORK

Room temperature co-fired tungsten metallization thermal diffusivity measurement experiments have been conducted for two types of geometric samples. The first, a through plane measurement normal to the metallization planes, proved unsuccessful due to technique limitations. The second, an in-plane measurement, with metallization planes parallel to the laser pulse heat flow, provided excellent fidelity. The results of this technique provided an average thermal conductivity (TC) of 99 W/mK. While only two samples were measured, they represented a random distribution of many individual diced sections. The technique was also successfully validated against a 13/73/13 CMC laminate metal heat spreader using the same in-plane fabrication methodology. A detailed uncertainty budget was not performed but it is assumed a 10~15% uncertainty should be expected. Scanning electron microscopy measurement of the metallization thickness had a first order effect on the calculated TC values. To the author's best knowledge this represents the first published TC data for co-fired refractory metallization.

The in-plane measurements were also compared against the theoretical TC prediction using the Wiedemann-Franz law. The theoretical value calculated had a conservative ten percent difference from measured results. Fundamental to the law is the proportion relationship that exists between electrical and thermal conductivity in metals. It has been the author's experience that 4-pt metallization resistivity measurements are more easily obtained and thus merit this estimation approach. Of course, numerous and more varied types of co-fired metallization measurements will need to be correlated before this estimation technique can be conclusively established.

As mentioned previously, infinite contact conductance was assumed for the in-plane FE model material interface. Qualitative evidence to support this assumption was seen with the close correlation between the homogenized model approach and measured results. Additionally, metallurgical inspection of the alumina/metallization interface will shown an absence of different glass or metal phases and/or impurities. The is not always the case with other thick film metallization systems, such as the sintering of Mo-Mn metallization onto previously fired (or densified) alumina ceramic.

The afore mentioned experiments provide a solid foundation for future experimental work. Those will include measurement of actual via-in-sample array geometries. The plane measurements should provide context as via barrel misalignment between ceramic layers will contribute to experimental error. It is also presumed the via metallization thermal conductivity will be decreased by as much as 50% due to increased electrical resistivity. This a consequence of reduced viscosity needed to fill small diameter vias before co-firing the ceramic substrate.

ACKNOWLEDGMENTS

The author would like to acknowledge Kyocera America multilayer manufacturing team for material support during this project. Additional acknowledgement is given to the F/A lab for hours of tedious sample fabrication.

REFERENCES:

1. Winser, M., "A Single package X-Band T/R module," *35th European Microwave Conference Vol. 1: Session EuM23 Module Packaging*, (2005) pp. 493-496.

2. Eblen, Mark, Takeshita Nobuo, Kim Franklin, "Thermomechanical Finite Element Techniques in Multilayer Ceramic Package Design," *Proc. 42nd International Symposium on Microelectronics,* San Jose, CA. Nov., (2009) pp. 268-274

3. Twentyman, M. E., "High-Temperature Metallizing Part 1: The Mechanism of Glass Migration in the Production of Metal-Ceramic Seals," *Journal of Material Science,* Vol. 10, No. 5, (1975), pp. 765-776.

4. Franz, R., Wiedemann, G., "Ueber die Wärme-Leitungsfähigkeit der Metalle," *Annalen der Physik* (in German) Vol. 165, No. 8 (1853), 497–531

5. Kittle, Charles, (1976) *Introduction to Solid State Physics.* 5th ed. pp. 143-150. New York: John Wiley & Sons.

6. Parrott, J.E., Stuckes, Audry D., (1975) *Thermal Conductivity of Solids*. pp. 143-150. New York: Methuen, Inc.

7. ASTM E1461-11, (2011) "Standard Test Method for Thermal Diffusivity of Solids by the Flash Method," *ASTM International*, West Conshohocken, PA, 2008.

8. Parker, W. J., Butler, C. P., Abbott, G. L., "Flash Method of Determining Thermal Diffusivity Heat Capacity and Thermal Conductivity," *Journal Applied Physics*, Vol. 32, No. 9, (1961) pp. 1679-1684.

9. Carslaw, H. S., Jaeger, J. C., (1959) *Conduction of Heat in Solids*. 2nd ed. p.101. New York: Oxford University Press.

10. Maglić, K. D., Cezairliyan, A., Peletsky, V. E., (1992) *Compendium of Thermophysical Property Measurement Methods Vol. 2: Recommended Measurement Techniques and Practices*. p. 284. New York, NY: Plenum Press.

11. Enck. R. C., Harris, R. D., Youngman, R. A., "Measurement of the Thermal Diffusivity of Translucent Aluminum Nitride," *Advanced Characterization Techniques for Ceramics*, W. Young editor, (Ceramic Transactions Vol. 5), American Ceramic Society, Westerville OH, (1989), pp. 214-222.

12. Taylor, R. E, "Thermal Conductivity Determinations of Thermal Barrier Coatings," *Materials Science and Engineering: A*, Vol. 245, No. 2 (1998) pp. 160-167.

13. Schimmel Jr. W. P., Beck J. V., Donaldson, A.B., "Effective Thermal Diffusivity for a Multimaterial Composite Laminate," *Journal of Heat Transfer,* Vol. 99, No. 3, (1977) pp. 466-470.

14. Taylor, R. E., Jortner, J., Groot, H., "Thermal Diffusivity of Fiber-Reinforced Composites Using the Laser Flash Method," *Carbon*, Vol. 23, No. 2, (1985) pp. 215-222.

15. Taylor, R. E., Kelsic, B. H., "Parameters Governing Thermal Diffusivity Measurements of Unidirectional Fiber-Reinforced Composites," *Journal of Heat Transfer,* Vol. 108, No. 1 (1986) pp. 161-165.

16. Balageas, D. L., Luc, A. M., "Transient Thermal Behavior of Directional Reinforced Composites: Applicability Limits of Homogeneous Property Model," *AIAA Journal*, Vol. 24, No. 1, (1986) pp. 109-114.

17. Alvarado, C. M., (1993) "*The Role of the Thermal Contact Conductance in the Interpretation of Laser Flash Data in Fiber-Reinforced Composites*," M.S. Theses, Department of Mechanical Engineering, Virginia Polytechnic Institute and State University.

18. Depalma, Carlos M., Private communication, 2011.

19. Depalma, C. M. A., Bhatt, H. D., Donaldson, K. Y., Hasselman D. P. H., Thomas, J. R., Hurst II E. P., "Role of Interfacial Thermal Barrier in the Measurement of the Longitudinal Thermal Conductivity of a Uniaxial Fiber-Reinforced Composite by the Flash Method," *Thermal Conductivity 22*, Timothy Tong ed., (1994) pp. 301-312.

20. ANSYS software, Releases 13.0-14.5, ANSYS Inc., Canonsburg, PA.

21. Sheikh, M. A., Taylor, S. C., Hayhurst, D. R., Taylor, R., "Measurement of Thermal Diffusivity of Isotropic Materials Using Laser Flash Method and its Validation by Finite Element Analysis," *Journal of Physics D*: Applied Physics, Vol. 33, No. 12 (2000) pp. 1536-1550.

22. Sandwell, Roger., email correspondence, LightMachinery, 2005.